Defects in III-N LEDs: experimental identification and impact on electro-optical characteristics

PROCEEDINGS OF SPIE

SPIEDigitalLibrary.org/conference-proceedings-of-spie

Defects in III-N LEDs: experimental identification and impact on electro-optical characteristics

Buffolo, Matteo, Roccato, Nicola, Piva, Francesco, De Santi, Carlo, Brescancin, Riccardo, et al.

Matteo Buffolo, Nicola Roccato, Francesco Piva, Carlo De Santi, Riccardo Brescancin, Claudia Casu, Alessandro Caria, Kalparupa Mukherjee, Camille Haller, Jean Francois Carlin, Nicolas Grandjean, Marco Vallone, Alberto Tibaldi, Francesco Bertazzi, Michele Goano, Giovanni Verzellesi, Mauro Mosca, Gaudenzio Meneghesso, Enrico Zanoni, Matteo Meneghini, "Defects in III-N LEDs: experimental identification and impact on electro-optical characteristics," Proc. SPIE 12022, Light-Emitting Devices, Materials, and Applications XXVI, 120220G (3 March 2022); doi: 10.1117/12.2606599

SPIE.

Event: SPIE OPTO, 2022, San Francisco, California, United States

2. BASIC PROPERTIES OF SEMICONDUCTOR DEFECTS

From an operating perspective, the impact that a semiconductor trap has on the functionality of the optoelectronic device that embeds it can mostly be described in terms of its optical and thermal capture/emission rates. These quantities define the rates at which carriers are exchanged between the energy levels associated to the traps and the bands of the semiconductor material, thus allowing to estimate the impact that the presence of the trap has on both the dynamic and static electro-optical characteristics of the devices. If we consider the typical relations for electron (or hole) thermal capture rates [1], we can see that the defect under consideration can be entirely described in terms of its capture cross-section $\sigma_{n,p}$, its thermal activation (or binding) energy E_a, its degeneracy and its concentration N_t. From a steady-state recombination standpoint, these parameters are of primary importance for determining the optical efficiency of a semiconductor emitter, since they determine the Shockley-Read-Hall (SRH) recombination rate in given bias scenario. The classical SRH theory in low injection regime and for an intrinsic semiconductor [2,3] shows that the SRH lifetime can be expressed as:

$$\tau_{srh} = \tau_0 \left[1 + \cosh\left(\frac{E_t - E_{fi}}{k_B T}\right)\right] \quad with \quad \tau_0 = \frac{1}{N_t \upsilon_{th} \sigma_{n,p}} \tag{1}$$

where υ_{th} is the thermal velocity of the carrier, k_B is the Boltzmann constant, $E_t - E_{fi}$ is the energy difference between the trap level and the intrinsic Fermi level, and where we have also assumed equal thermal velocities for electrons and holes, and that $\sigma_n = \sigma_p$. If we consider different types of defects present in equal concentrations, Equation (**1** shows that the most detrimental in terms of SRH recombination would be the ones that either have larger capture cross-section, or higher activation energy, the latter term being more relevant since the SRH lifetime has an exponential dependence on it. The dependence of the A recombination coefficient (SRH recombination rate, measured in s^{-1}), which is equivalent to the inverse of the SRH lifetime, is evidenced by the color-coded map reported in the background of Figure 1.

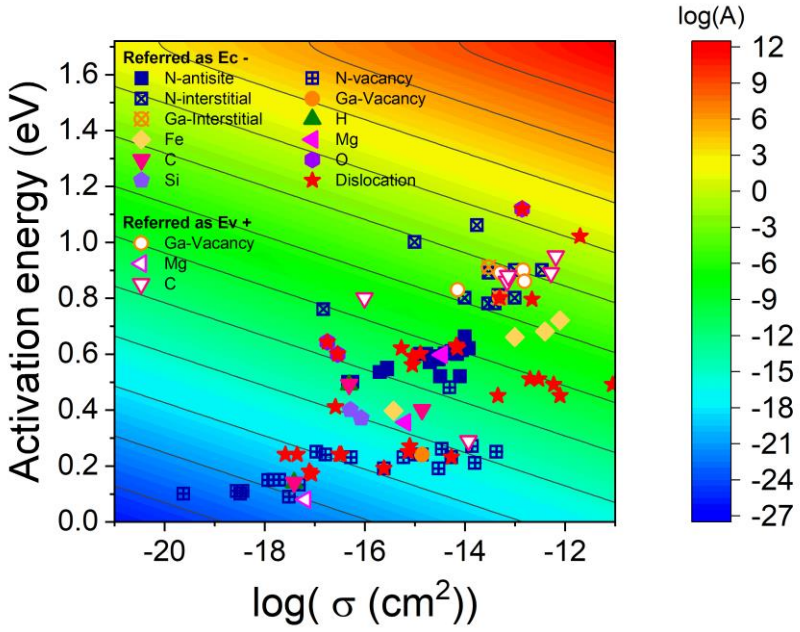

Figure 1. Experimentally determined thermal activation energies plotted against apparent capture cross sections of reported traps in GaN. The underlying heat-cool color-coded map reports the value of the A coefficient (SRH recombination rate) calculated through Equation (**1**, for $N_t = 10^{16}$ cm^{-3} at T = 300 K. For a more complete database on GaN-related traps the reader can refer to [4].

On this plot we have also reported the experimentally-determined values for the activation energy and the apparent capture cross-section of common traps detected on GaN-based devices. The main parameters of these traps, as well as their position within the bandgap of GaN, are reported in Table 1 and depicted by Figure 2.

Table 1 Summary of the experimentally-determined characteristics of the most common traps in GaN

Type of defect	$\Delta E = E_T - E_{fi}$ (eV)	Capture cross section (cm^2)
Native defects		
Ga_I	+0.81 to +0.92	~ 10^{-14}
V_{Ga}	+0.60, +1.08, +1.12, +1.48, and from -0.86 to -0.89	$2.6 \cdot 10^{-16}$ to $5.5 \cdot 10^{-13}$
N_{Ga}	+1.05 to +1.2	$1 \cdot 10^{-16}$ to $2.3 \cdot 10^{-13}$
V_N	+1.45 to +1.63	$2.4 \cdot 10^{-20}$ to $1.4 \cdot 10^{-14}$
N_I	+0.66 to +0.96	$1.5 \cdot 10^{-17}$ to $1 \cdot 10^{-13}$
Extended defects	+0.60 to +1.55	$8.7 \cdot 10^{-18}$ to $2 \cdot 10^{-12}$
Impurities-related defects		
Si	+0.59, +0.4, +0.37	~ 10^{-17}
O	+0.60 to + 1.21	$2.9 \cdot 10^{-17}$ to $1.4 \cdot 10^{-13}$
Mg	+1.12, +1.36, -1.64	$6.6 \cdot 10^{-18}$ to $3.5 \cdot 10^{-15}$
C	+1.23 to 1.58, and from -0.77 to -1.43	$3.9 \cdot 10^{-18}$ to $6.7 \cdot 10^{-13}$
Fe	+1 to +1.32	$3.8 \cdot 10^{-16}$ to $1 \cdot 10^{-13}$
H	+1.23, and +1.58	$2.6 \cdot 10^{-16}$ to $9 \cdot 10^{-13}$

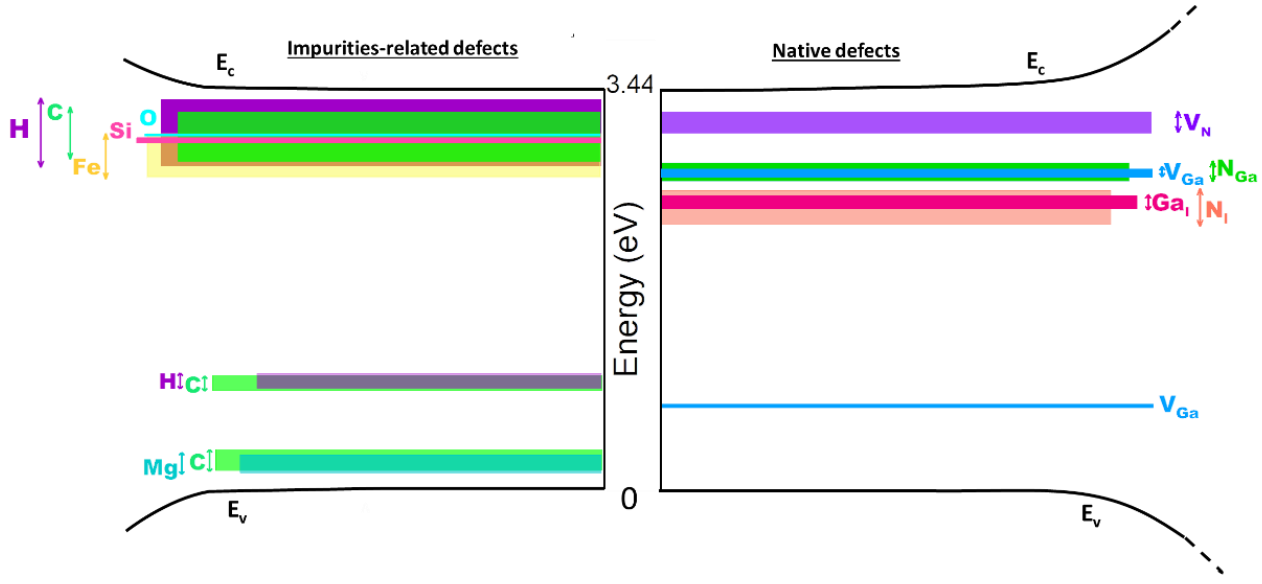

Figure 2. Energy position of common GaN-related traps within the bandgap of the semiconductor material.

Groups of traps placed toward the upper right corner of Figure 1, i.e. featuring a larger capture cross section and higher activation energy, are the most critical for the optical efficiency of the device, if we consider SRH recombination to be the dominant non-radiative recombination process within the active region of the device. In the view, the reported database indicates that the most detrimental types of defects for GaN emitters may include carbon-, N_i- , Fe- and V_{Ga}-related traps, in addition to some extended defects and oxygen complexes.

The properties of a semiconductor defect are not solely determined by the physical quantities that allow to describe its thermal capture, or emission, processes. If we consider optically-assisted capture and emission processes, also the determination of the (electron or hole) optical capture cross section $\sigma_{n,p}^{o}$ of the defect becomes relevant. The dependence of this parameter on photon energy is of particular interest, since it allows to determine a first-order sketch of the configurational coordinate CC) diagram of the deep level [5].

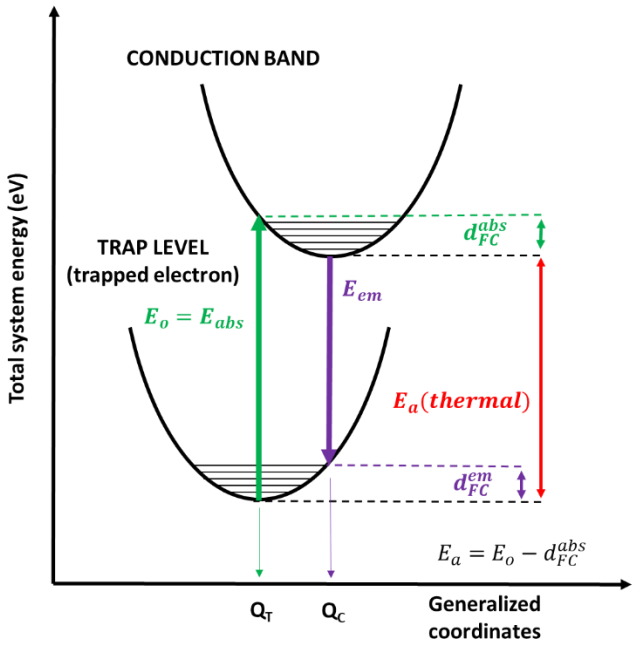

Figure 3. Sketch of the generalized configurational coordinate diagram showing the possible photon-assisted transitions between an electron trap level and the conduction band.

This kind of diagram, here reported in Figure 3 for the case of an electron trap located below the conduction band, aims at representing the total system energy in function of a generic set of coordinates Q: these coordinates can be thought to represent the average distance between the lattice atoms located in proximity of the defect [6]. Since the capture/release of a carrier by the defective site changes the local density of charge, as a consequence to this process the lattice atoms have to re-arrange their relative distances to reach a more energetically favorable configuration. In a CC diagram this re-arrangement corresponds to a shift in the energy minimum of the E-Q relation of the trapped carrier (Q_T) with respect to the position of E-Q relation of a carrier within the conduction band (Q_C). According to the Franck-Condon principle, optical transitions are much faster than the lattice relaxation time [7], therefore optically-induced transitions do not induce a variation in Q. This indicates that i) the photon-assisted emission of a carrier from a deep level follows a "vertical" path on the CC diagram (see the green arrow in Figure 3) and ii) that the newly promoted carrier within the CB does not occupy a position of minimum energy, and its excess energy is released to the lattice in the form of heat (multiphonon emission, MPE). This amount of energy, corresponding to the difference between the minimum optical ionization energy (E_O) and the thermal ionization energy of the level, i.e. its activation energy, is called Franck-Condon shift, and is typically referred to as d_{Fc} [8]. The estimation of the Franck-Condon shift can be performed by measuring the dependency of the optical capture cross section on photon energy, and by performing an appropriate fitting of the experimentally determined photoionization cross-section (PCS) spectrum [8]. A first-order approximation of the CC diagram can then be obtained once

both d_{Fc} and E_a (or alternatively E_O) are known. If numerically consistent and accurate, an approximated sketch of the CC diagram of a deep level can ease the description of specific capture processes, such as carrier capture assisted by multi-phonon emission [9], but also allow the explanation of peculiar defects-related physical properties of semiconductor materials, such as the persistent photoconductivity induced by DX centers in GaAs [5].

3. IMPACT OF INDIUM-RELATED DEFECTS

We have previously demonstrated that defects are detrimental for the optical efficiency of semiconductor emitters, as they can act as efficient non-radiative recombination centers, thus preventing radiative recombination within the quantum wells of the LED, or favoring the loss of injected carriers before they can reach the active volume. Since high-quality InGaN layers are required to successfully manufacture devices emitting at longer wavelengths, a great interest is directed toward the analysis of In-related defects. The epitaxial growth of high indium content layers is critical, because with increasing In molar fraction i) the lattice mismatch with respect to the adjacent GaN barriers increases, thus increasing lattice strain, ii) the segregation of defects located at the GaN surface is favored [10]. In both cases, the increase in In molar fraction tends to favor the increase in local concentration of NRRCs that can lower the optical efficiency of the devices. The aforementioned segregation of defects in In-rich layers can be exploited for increasing the material quality of the active layer by employing an highly-doped InGaN/GaN underlayer (UL) placed below the multi quantum wells (MQWs) region [11,12].

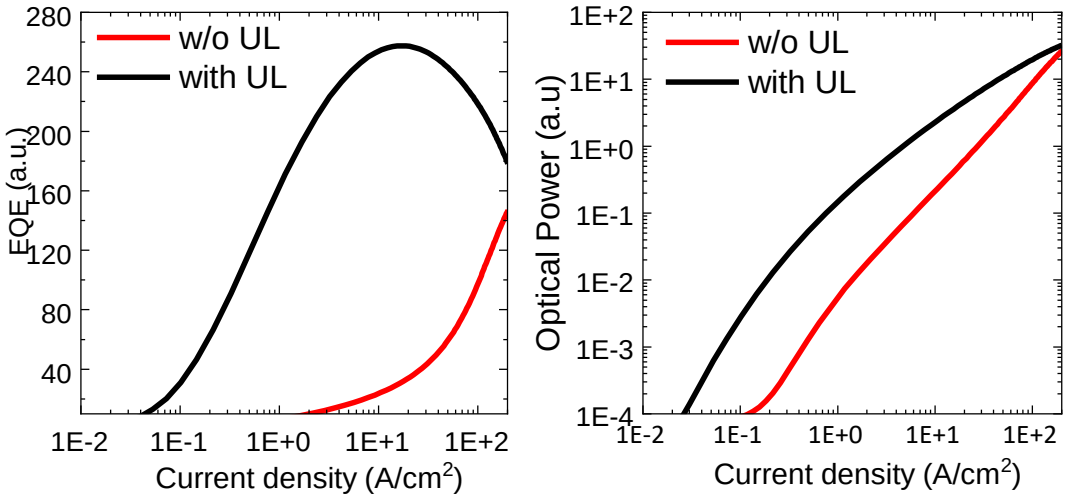

(a) (b)

Figure 4. (a) Comparison of the EQE and (b) of the optical emission as a function of current density between two InGaN/GaN LEDs with and without SL UL (10% In, 2.7 nm QW width).

Figure 4 highlights the strong effect that the InGaN UL has on the optical efficiency of visible InGaN/GaN LEDs: a measurable increase in the external quantum efficiency (EQE) within the typical operating regime of the LED is clearly visible, and the advantage becomes even more evident at lower injection levels, where the contribution of SRH recombination to the overall rate of recombination is much higher.

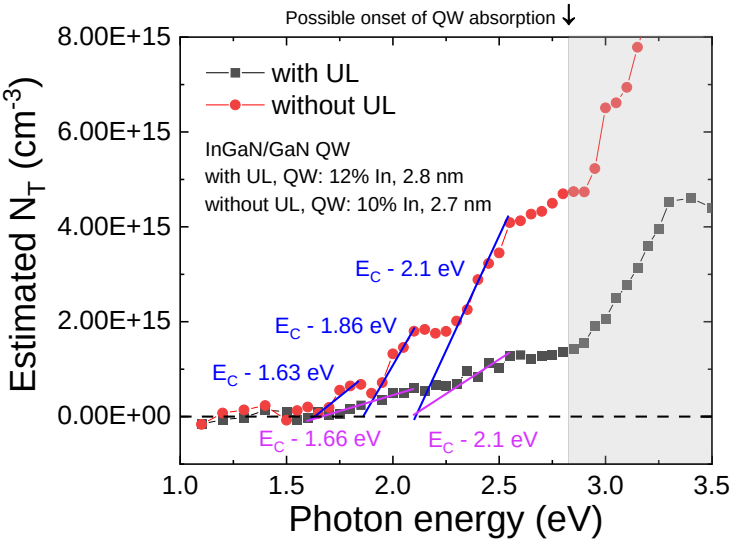

Figure 5. Comparison between steady state photo-capacitance measurements of InGaN LEDs with and without UL. The thermal ionization energy levels have been extracted from PCS spectra fitted by means of the Pässler model [8]. The solid lines indicate the changes in slope of the SSPC signal, each corresponding to the optical response of a different defect level (or of other optical absorptive regions, like the QWs or the GaN layers included within the space-charge region (SCR)). The greyed out area indicates the photon energy range where possible absorption and e-h pairs generation by the QW may occur.

To pinpoint the physical origin of the In-related defects, deep-level optical transient spectroscopy (DLOS) measurements have been carried out on devices with and without the UL. The results of this analysis, here summarized by the plot in Figure **5**, indicate that i) defects concentration within, and in proximity of the active region of the LED featuring the InGaN UL is lower with respect to the device without the UL, and ii) that similar defects are detected in both samples. These results prove the efficacy of the InGaN UL as a defect-filtering layer, and show that its introduction does not lead to the generation of new defect species [11].

To further prove the impact of the UL on the concentration of defects within the active region, DLOS and lighted capacitance-voltage characterizations (L-CV) [13] have been carried out on a set of devices featuring a similar epitaxial structure, which differed only in terms of the In molar fraction within the QW (the sketch of the structure is reported by the left image in Figure 6). The estimated defect concentration within the active region and the UL are reported in the right plot of Figure 6. The estimation was obtained by measuring the difference in voltage, for a given device capacitance, of the LED in dark and under illumination with a photon energy of 2.3 eV: according to the results reported in Figure **5**, this energy is sufficient to allow the detrapping of all the detectable defect species within the SCR of the device.

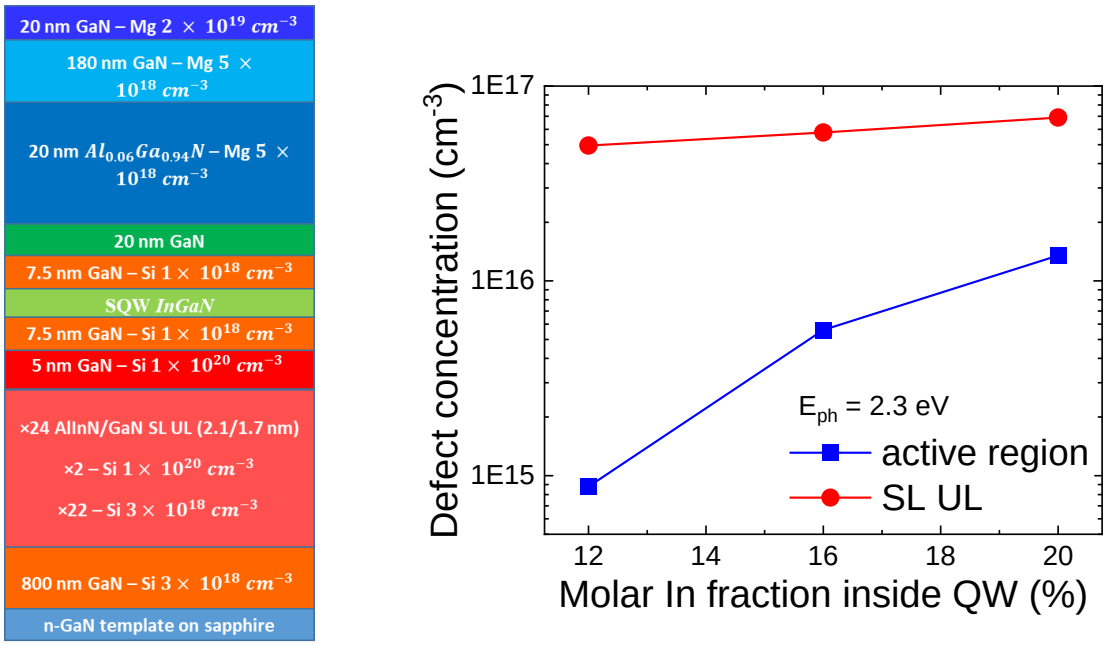

Figure 6. (left) Structure of the three samples under investigation. The devices share the same epitaxial structure, while differing in terms of In content within the quantum well. The indium content is 12%, 16%, 20% for the wafers named A, B and C, respectively. (right) Estimation of the average defect concentration inside the two probed regions (the "active region" corresponds to the volume including QWs, barriers and the spacer) carried out through lighted-CV measurements at a photon energy $E_{ph} = 2.3\ eV$. The density of defects is nearly identical within the UL for the three wafers, whereas it increases significantly with indium content in the active region.

The experimental data demonstrate that defects density within the active region increases monotonically with indium molar fraction, confirming that alloys with higher In content tend to incorporate higher concentration of defects; also, defect density in the QWs is significantly lower than in the InGaN SL, since defects are incorporated in the underlayer. Finally, the density of defects in the SL is similar across the three samples, which confirms an high reproducibility of the growth process for that specific layer.

Regarding the physical origin of the In-related defects acting as NRRCs, multiple theories are under debate. One of these considers that native GaN defects, possibly V_N, are generated in correspondence of the surface of the material during high temperature growth. These defects are then believed to interact with the In atoms belonging to the QW, thus forming complexes that may act as luminesce killer centers [10,14]. Another theory [15,16] correlates the presence of such defects with threading dislocations (TDs), which are supposed to interact with In atoms and to form NRRCs in In-rich layers. Finally, a tentative association of In-related NRRCs to V_N-V_{III} divacancies was proposed by the authors in [10,17].

4. TRAP-ASSISTED TUNNELLING IN INGAN LEDS

In the previous paragraphs we have focused our attention on the impact that defects, and especially In-related defects, can have on the optical efficiency of InGaN LEDs . However, the presence of shallow or deep levels can also impact on the carrier transport mechanisms, especially easing defect-assisted tunneling processes in low forward bias conditions [18,19]. To quantitatively evaluate the impact that deep-levels have on the low-forward bias conduction in InGaN/GaN LEDs, Sentaurus TCAD simulations, assisted by defects spectroscopy techniques and I-V measurements, have been employed to model the electrical behavior of the devices featuring the epitaxial structure reported in Figure 6. On the basis of the experimentally-determined defect distribution, I-V characteristic, and theoretical structure, a Sentaurus device model for the LEDs under investigation has been created. The simulated equilibrium band diagram in proximity of the active region of the implemented structure is reported in Figure 7.

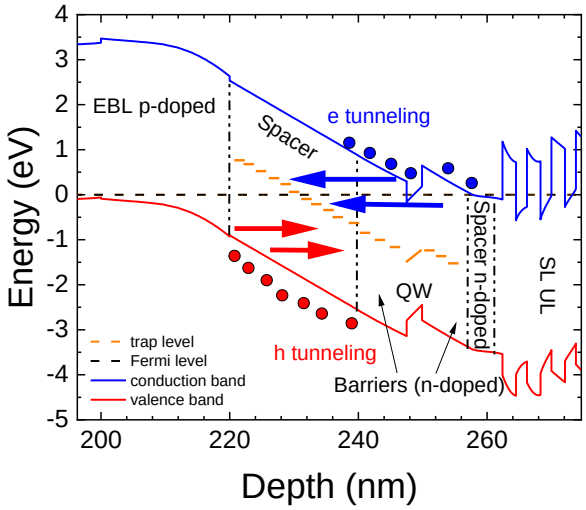

Figure 7. Simulated band diagram at thermal equilibrium of sample C, showing a schematic representation of the implemented TAT process. The electrons tunnel toward the near-midgap traps from the highly doped spacer layer at the n-side, whereas the holes tunnel from the p-side. Only the E_c-1.67 eV level, which is the most relevant for the TAT, is shown (a slight variation in the band-to-trap alignment is expected to occur in low forward bias, where TAT is relevant, with respect to the thermal equilibrium condition shown above).

Careful tuning of the simulations parameters, based on the experimentally determined properties of the deep levels detected within the active region, allowed us to find that i) among the two defects detected by the DLOS measurement at E_c-1.29 eV and E_c-1.67 eV, the latter (and deeper) is the one mainly determining the entity of the TAT-related current; ii) that only defects positioned within the undoped spacer region effectively contribute to the tunneling process, which reveals that an aging-induced increase in the forward leakage current of LEDs featuring a similar epitaxial structure can be directly related to an increase in the concentration of deep levels within this particular layer.

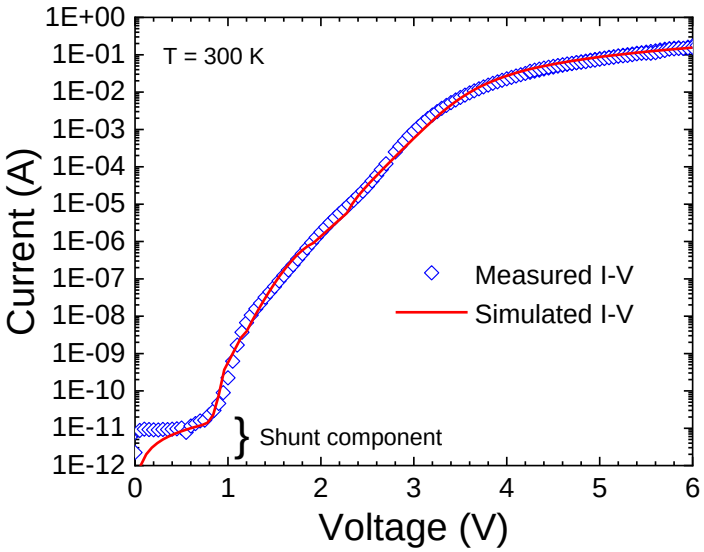

Figure 8. Comparison between the experimental and the simulated I-V characteristic for a single QW InGaN LED with 20% In within the QW (sample C).

The final tuning of the model, based on experimentally-determined defects placement and properties, allowed us to obtain a very good matching between the experimental I-V curve of the sample, reported by the dots in Figure 8, and the simulated trend of the electrical characteristic, reported in red.

5. DEFECT-RELATED DEGRADATION

Electrical and optical performance are not the sole device characteristics that can be influenced by the presence of defects, since also reliability depends on the crystalline quality of the semiconductor layers that form the device. Unwanted deep levels or trap states can promote the local accumulation of charge that induces the formation of potential barriers [20], or further promote the generation of non-radiative recombination centers through recombination-enhanced processes [21–23]: in both cases, an high pre-existing density of defects within the device can drastically limit its long-term reliability. To evaluate this aspect, a set of current step-stress tests have been carried out on the series of SQW devices described in Figure 6, which were only differing in terms of In-content within the QW. Since we have previously shown that higher In content within the QW corresponds to an higher density of defects within the active region, this test has the specific goal to pinpoint whether an initial higher device defectiveness can lower its expected lifetime.

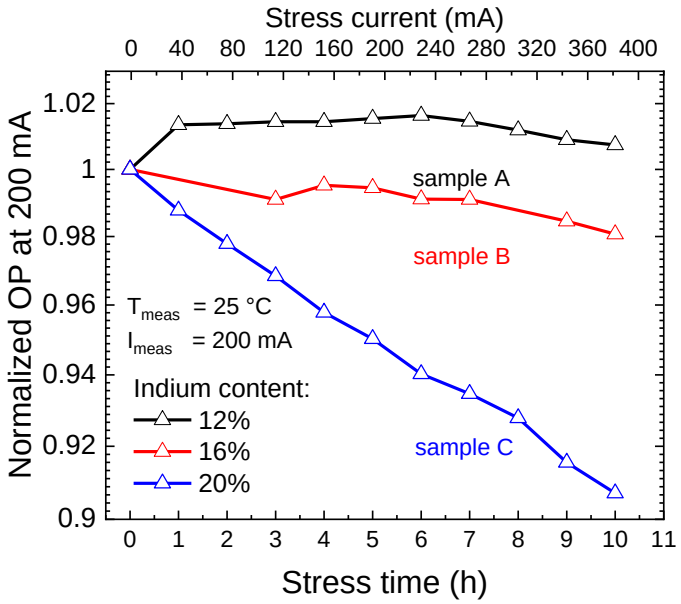

Figure 9. Degradation of the optical power measured at 200 mA after each cycle of the current step-stress experiment. A stronger degradation for LEDs featuring higher In content in the QW can be observed.

The results of the tests are summarized by the plot in Figure 9, which reports the decay of the OP measured at the LED nominal current after each stress step. The experimental data clearly indicate that the OP decay rate at high measuring injection levels is strictly dependent on In concentration within the well. A first explanation for this behavior considers the role of charge/defects generation and/or propagation in the reduction of the injection efficiency of the device [24]. Specifically, charged defects located in proximity of the QW can act as scattering centers or form potential barriers that can ultimately lower the capture rate from the QW. The strong reduction in OP at high injection levels can also be interpreted as a relative increase in the defect-assisted Auger recombination [25], whose rate strongly depends on defect concentration and can overcome radiative recombination. Both these processes would be stronger within a device with higher initial defect concentration, due to their dependence on N_t. Similarly, also the degradation rate would be faster in devices featuring higher In concentration, since the reduced radiative efficiency of GaN LEDs emitting at longer wavelengths may favor recombination-enhanced degradation and/or diffusion processes [21,23,26]. Details on defects in GaN can also be found in [27].

6. CONCLUSIONS

In conclusion, with this paper we have investigated the impact of semiconductor defects on the electro-optical performance and reliability of III-N visible LEDs. After highlighting which are the most detrimental types of GaN-related defects in terms of SRH recombination, we have shown by means of an extensive set of characterization techniques that devices featuring In-rich QWs exhibit higher defects density and faster degradation rates. We have also shown that the insertion of an InGaN UL below the active region can efficiently reduce the density of defects within the active region by acting as a segregation/filtering layer. Finally, we have shown that deep levels located within the GaN spacer near the p-side contribute to the forward TAT current of the LEDs, further indicating that defect properties, including their spatial location, contribute in determining their specific effect on the functionality of the devices.

ACKNOWLEDGEMENTS

This research was partly performed within project INTERNET OF THINGS: SVILUPPI METODOLOGICI, TECNOLOGICI E APPLICATIVI, co-founded (2018-2022) by the Italian Ministry of Education, Universities and Research (MIUR) under the aegis of the "Fondo per il finanziamento dei dipartimenti universitari di eccellenza" initiative (Law 232/2016).

REFERENCES

[1] Mooney, P. M., "Chapter 2 Defect Identification Using Capacitance Spectroscopy," Semicond. Semimetals **51**, 93–152 (1999).

[2] Muller, R. S., Kamins, T. I. and Chan, M., [Device Electronics for Integrated devices], John Wiley & Sons (2002).

[3] Meneghini, M., De Santi, C., Tibaldi, A., Vallone, M., Bertazzi, F., Meneghesso, G., Zanoni, E. and Goano, M., "Thermal droop in III-nitride based light-emitting diodes: Physical origin and perspectives," J. Appl. Phys. **127**(21), 211102 (2020).

[4] Meneghini, M., De Santi, C., Abid, I., Buffolo, M., Cioni, M., Khadar, R. A., Nela, L., Zagni, N., Chini, A., Medjdoub, F., Meneghesso, G., Verzellesi, G., Zanoni, E. and Matioli, E., "GaN-based power devices: Physics, reliability, and perspectives," J. Appl. Phys. **130**(18), 181101 (2021).

[5] Alkauskas, A., McCluskey, M. D. and Walle, C. G. Van de., "Tutorial: Defects in semiconductors—Combining experiment and theory," J. Appl. Phys. **119**(18), 181101 (2016).

[6] Reshchikov, M. A., "Measurement and analysis of photoluminescence in GaN," J. Appl. Phys. **129**(12), 121101 (2021).

[7] Chantre, A., Vincent, G. and Bois, D., "Deep-level optical spectroscopy in GaAs," Phys. Rev. B **23**(10), 5335 (1981).

[8] Pässler, R., "Photoionization cross-section analysis for a deep trap contributing to current collapse in GaN field-effect transistors," J. Appl. Phys. **96**(1), 715 (2004).

[9] Alkauskas, A., Yan, Q. and Van De Walle, C. G., "First-principles theory of nonradiative carrier capture via multiphonon emission," Phys. Rev. B **90**, 75202 (2014).

[10] Haller, C., Carlin, J. F., Jacopin, G., Liu, W., Martin, D., Butté, R. and Grandjean, N., "GaN surface as the source of non-radiative defects in InGaN/GaN quantum wells," Appl. Phys. Lett. **113**(11), 111106 (2018).

[11] Piva, F., De Santi, C., Caria, A., Haller, C., Carlin, J. F., Mosca, M., Meneghesso, G., Zanoni, E., Grandjean, N. and Meneghini, M., "Defect incorporation in In-containing layers and quantum wells: experimental analysis via

deep level profiling and optical spectroscopy," J. Phys. D. Appl. Phys. **54**(2), 025108 (2020).

[12] Armstrong, A. M., Bryant, B. N., Crawford, M. H., Koleske, D. D., Lee, S. R. and Wierer, J. J., "Defect-reduction mechanism for improving radiative efficiency in InGaN/GaN light-emitting diodes using InGaN underlayers," J. Appl. Phys. **117**(13), 134501 (2015).

[13] Armstrong, A., Henry, T. A., Koleske, D. D., Crawford, M. H. and Lee, S. R., "Quantitative and depth-resolved deep level defect distributions in InGaN/GaN light emitting diodes," Opt. Express **20**(S6), A812 (2012).

[14] Haller, C., Carlin, J. F., Jacopin, G., Martin, D., Butté, R. and Grandjean, N., "Burying non-radiative defects in InGaN underlayer to increase InGaN/GaN quantum well efficiency," Appl. Phys. Lett. **111**(26), 262101 (2017).

[15] Armstrong, A., Henry, T. A., Koleske, D. D., Crawford, M. H., Westlake, K. R. and Lee, S. R., "Dependence of radiative efficiency and deep level defect incorporation on threading dislocation density for InGaN/GaN light emitting diodes," Appl. Phys. Lett. **101**(16), 162102 (2012).

[16] Armstrong, A. M., Crawford, M. H. and Koleske, D. D., "Contribution of deep-level defects to decreasing radiative efficiency of InGaN/GaN quantum wells with increasing emission wavelength," Appl. Phys. Express **7**(3), 032101 (2014).

[17] Chichibu, S. F., Uedono, A., Kojima, K., Ikeda, H., Fujito, K., Takashima, S., Edo, M., Ueno, K. and Ishibashi, S., "The origins and properties of intrinsic nonradiative recombination centers in wide bandgap GaN and AlGaN," J. Appl. Phys. **123**(16), 161413 (2018).

[18] Mandurrino, M., Verzellesi, G., Goano, M., Vallone, M., Bertazzi, F., Ghione, G., Meneghini, M., Meneghesso, G. and Zanoni, E., "Physics-based modeling and experimental implications of trap-assisted tunneling in InGaN/GaN light-emitting diodes," Phys. Status Solidi Appl. Mater. Sci. **212**(5), 947–953 (2015).

[19] Roccato, N., Piva, F., Santi, C. De, Brescancin, R., Mukherjee, K., Buffolo, M., Haller, C., Carlin, J.-F., Grandjean, N., Vallone, M., Tibaldi, A., Bertazzi, F., Goano, M., Verzellesi, G., Meneghesso, G., Zanoni, E. and Meneghini, M., "Modeling the electrical characteristics of InGaN/GaN LED structures based on experimentally-measured defect characteristics," J. Phys. D. Appl. Phys. **54**(42), 425105 (2021).

[20] Strauss, U., Lermer, T., Müller, J., Hager, T., Brüderl, G., Avramescu, A., Lell, A. and Eichler, C., "Study of defects and lifetime of green InGaN laser diodes," Phys. Status Solidi Appl. Mater. Sci. **209**(3), 481–486 (2012).

[21] Kimerling, L. C., "Recombination enhanced defect reactions," Solid State Electron. **21**(11–12), 1391–1401 (1978).

[22] Mukherjee, K., Selvidge, J., Jung, D., Norman, J., Taylor, A. A., Salmon, M., Liu, A. Y., Bowers, J. E. and Herrick, R. W., "Recombination-enhanced dislocation climb in InAs quantum dot lasers on silicon," J. Appl. Phys. **128**(2), 025703 (2020).

[23] Uematsu, M. and Wada, K., "Recombination-enhanced impurity diffusion in Be-doped GaAs," Appl. Phys. Lett. **58**(18), 2015–2017 (1991).

[24] Roccato, N., Piva, F., De Santi, C., Buffolo, M., Haller, C., Carlin, J. F. ois, Grandjean, N., Meneghesso, G., Zanoni, E. and Meneghini, M., "Effects of quantum-well indium content on deep defects and reliability of InGaN/GaN light-emitting diodes with under layer," J. Phys. D. Appl. Phys. **54**(50), 505108 (2021).

[25] David, A., Young, N. G., Lund, C. and Craven, M. D., "Review-The Physics of Recombinations in III-Nitride Emitters," ECS J. Solid State Sci. Technol., 9 (2020).

[26] Buffolo, M., Lain, F., Zenari, M., Santi, C. De, Norman, J., Bowers, J. E., Herrick, R. W., Meneghesso, G., Zanoni, E. and Meneghini, M., "Origin of the Diffusion-Related Optical Degradation of 1.3 μm Inas QD-LDs Epitaxially Grown on Silicon Substrate," IEEE J. Sel. Top. Quantum Electron. **28**(1) (2022).

[27] Meneghini, M., De Santi, C., Abid, I., Buffolo, M., Cioni, M., Khadar, R. A., Nela, L., Zagni, N., Chini, A., Medjdoub, F., Meneghesso, G., Verzellesi, G., Zanoni, E., and Matioli, E., "GaN-based power devices: Physics, reliability, and perspectives", Journal of Applied Physics 130, 181101 (2021)